LITERATURE CITED

1. Sherwood, T. K., P. L. T. Brian, R. E. Fisher, and L. Dresner, *Ind. Eng. Chem. Fundamentals*, **4**, 113 (1965).
2. Gill, W. N., Chi Tien, and D. W. Zeh, *Ind. Eng. Chem. Fundamentals*, **4**, 433 (1965).
3. ————, *Quart. Rept. Jan. 1, 1965-March 31, 1965*, Contract 14-01-0001-401, Office of Saline Water, U. S. Department of Interior.
4. Lighthill, M. J., *Proc. Roy. Soc. (London)*, **202A**, 359 (1950).
5. Gill, W. N., D. W. Zeh, and Chi Tien, "On Boundary Layer Effects in Reverse Osmosis Desalination," *Ind. Eng. Chem. Fundamentals*, in press.
6. Gill, W. N., Chi Tien, and D. W. Zeh, *Final Rept. July 1, 1964-June 30, 1965*, Contract 14-01-0001-401, Office of Saline Water, U. S. Department of Interior; *Intern. J. Heat Mass Transfer*, in press.
7. "Tables of The Incomplete Beta Function," K. Pearson, ed., Cambridge Univ. Press (1948).

Manuscript received October 6, 1965; revision received January 10, 1966; paper accepted January 12, 1966. Paper presented at A.I.Ch.E. Dallas meeting.

Film Boiling of Liquid Nitrogen from Porous Surfaces with Vapor Suction: Experimental Extensions

V. K. PAI and S. G. BANKOFF

Northwestern University, Evanston, Illinois

Previous work on film boiling of liquid nitrogen on flat horizontal porous surfaces with porous ceramic flow control elements is extended to tubular geometries and to very thin (asbestos paper) flow control members. At no loss in stability it is demonstrated that heat transfer coefficients more than five times greater than those in conventional film boiling can be obtained. An approximate model for a single liquid tongue breaking through the heating section at the critical flow rate is also presented. The upper (complete breakthrough) and lower (local breakthrough) limits on critical flow rate can be obtained theoretically. The experimental points lie between these two limits and, in general, are fairly close to the upper limit.

Methods for improving the heat transfer rate in both the stable boiling regimes (nucleate and film boiling) have been the subject of a number of investigations in recent years. These include the use of capillary wicking (*1* to 3), fixed nucleation sites (*4*, 5), impressed electrical fields (*6* to *9*), ultrasonic fields and pulsating pressures (*10* to *12*), and porous heating sources with vapor suction (*13* to *16*). The last mentioned mode of boiling heat transfer, with which the present work is concerned, provides the additional advantage of vapor superheat and the elimination of vapor binding in reduced gravitational fields.

The feasibility of film boiling* on an electrically heated horizontal porous plate with the vapor being sucked through the plate has been demonstrated in previous studies (*14, 15*). In order to stabilize the system, it was necessary to use a porous glass-bonded quartz block, 3/16 to 1½ in. thick, next to the heating element on the liquid side. In the absence of this element, strong pressure oscillations were recorded, followed by quenching of a portion of the heating element to the liquid temperature. Increases in heat transfer coefficients of about 2.5 times over those in normal film boiling were noted with vapor suction. Although the ceramic blocks were found to be well able to stabilize film boiling with vapor suction, the full advantages of this mode of heat transfer were not achieved. With no vapor suction, all the vapor was vented up through the ceramic blocks, resulting in considerably lower heat transfer coefficients. Change in porosity of the blocks was shown to have negligible effects on the heat transfer coefficient, although there existed a limiting porosity for effective flow control. It seemed therefore desirable to investigate other flow control elements over a wide range of heat fluxes. In the present work, film boiling of liquid nitrogen with vapor suction is studied on both flat and tubular porous heating elements at heat fluxes as high as 80,000 B.t.u./(hr.)(sq.ft.). A porous metallic plate, which is similar to the heating element and hence provides a compact sandwich construction, as well as thin asbestos papers, are used as flow control elements. Two different types of materials varying in thickness are used for the heating elements. In addition, an approximate theoretical model for liquid breakthrough is developed in the Appendix.

* Actually, none of the common boiling regime classifications fit the present system. The term *controlled-access film boiling* might be more properly descriptive, since at high suction rates it is thought that the flow control elements serve to distribute liquid uniformly to the hot porous surface. At sufficiently low flow rates, however, vaporization undoubtedly occurs principally in the flow control element.

V. K. Pai is at American Cyanamid Company, Stamford, Connecticut.

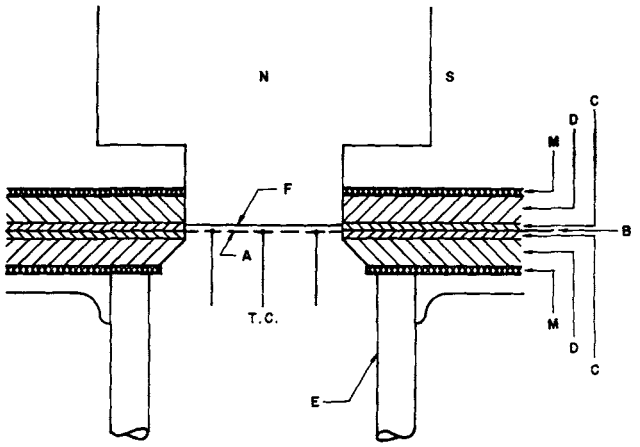

Fig. 1. Heat transfer cell with flat heating elements.

EXPERIMENTAL DESIGN

Two types of heating elements were used in the experiments: a two-layer composite of Rigimesh J, a 316 stainless steel screen with a wire count of 165 × 1,400 and an average pore diameter of 10μ, with a composite thickness of 0.013 in.; and a 1/32-in.-thick sintered porous stainless steel also with an average pore diameter of 10μ (abbreviated as PSS G). Rigimesh J tubes were prepared by rolling the sheet material to ½ in. I.D. and soldering the seam with silver solder. PSS G tubes were specially obtained and had an approximately 1/16-in.-wide welded seam. Rigimesh J is a relatively high resistance element and has greater strength at high temperatures than the sintered PSS G elements.

The heat transfer cell with flat heating elements, which is similar to the one used in the previous studies (*14, 15*), is sketched in Figure 1. The heating element (**A**), silver-soldered to copper strip leads (**B**), was sandwiched between two asbestos gaskets (**C**), two transite flanges (**D**), and two metal plates (**M**), and bolted to the flange of a 3-in. I.D. Pyrex exhaust pipe (**E**). Nonhardening Permatex gasketing cement was used as the sealing agent. A 6-in.-high pool of liquid nitrogen at atmospheric pressure (**N**) was maintained above the flow control element in a styrofoam container (**S**). The flow control element (**F**) was placed on top of the heating element and cemented on the sides with Saureisen No. 31 cement.

A cross-sectional view of the heat transfer cell with a vertically mounted tubular heating element is shown in Figure 2. The total length of the heating element (**A**) was 5 in. and the I.D. ½ in. Two copper rings (**B**) were soldered to the tube at its ends and were protected from the liquid by two transite flanges (**D**) cemented to the tube and the copper rings with Saureisen No. 31 cement. At the top end, the tube opening was closed by means of a copper disk (**C**) to which the transformer leads were welded. This assembly was insulated by a transite ring (**E**), a maranite cap (**F**), and a styrofoam enclosure (**G**). At the bottom end of the tube, a copper ring (**H**), carrying the transformer leads, was set-screwed to the copper flange (**B**) of the tube. A piece of aluminum foil (**I**) was also used to insure contact between the two copper pieces. This assembly was gasketed by asbestos (**J**) and bolted to a transite piece (**K**) and a metal plate (**L**). The Pyrex exhaust pipe was also bolted to this assembly. This nitrogen pool was provided by a styrofoam container (**GG**). Nonhardening Permatex cement was again used as the sealing agent. The flow control element (**P**) was a thin asbestos paper wrapped tightly around the tube and held in place by means of a Fiberglas thread and cement.

Two types of flow control elements were used: porous stainless steel (average pore diameter 65μ and approximately 50% porosity) plate ⅛ in. thick, which was separated from the heating element by a 1/64-in. layer of Fiberglas cloth for electrical insulation; and either a 1/16-in.-thick commercial grade asbestos paper, or more often a 0.01-in.-thick (Novabestos) glass-bonded asbestos paper.

The vapor exhaust system consisted of two calibrated rotameters and a vacuum pump. The pressure below the heating element which controlled the flow rate was measured with a manometer and the temperature of the exhaust pipe was measured with two chromel-alumel thermocouples located about 2 in. below the heater and shielded from radiation effects by a bed of ¼-in. berl saddles. The Pyrex exhaust pipe was also stuffed with glass wool.

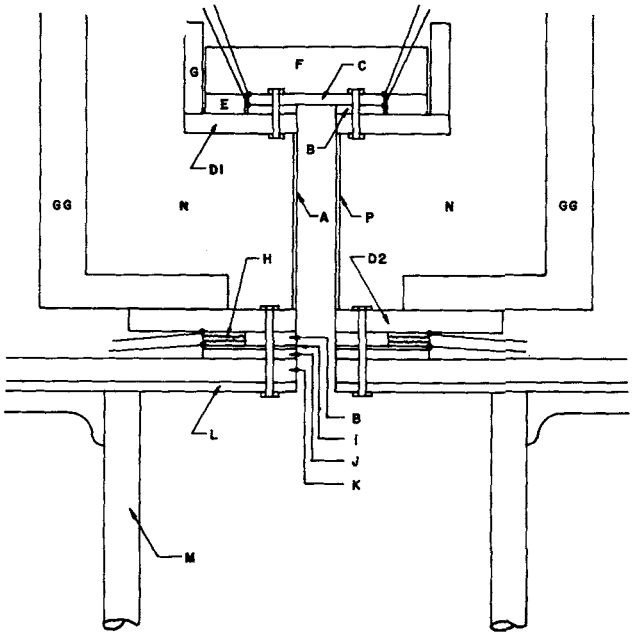

Fig. 2. Heat transfer cell with tubular heating elements.

The vapor suction through the porous heating element made it necessary to use the heating element itself as a resistance thermometer to obtain an accurate measurement of the surface temperature. In addition a number of chromel-alumel thermocouples were attached to the bottom of the heating element. The thermocouple data were used to make the correction for temperature distribution to ascertain whether any part of the heating element was quenched by liquid, which defined the end of the stable operation, and also in the calibration of resistance of the heating element. The locations of these thermocouples, along with the dimensions of the heat transfer surface, are shown in Figures 3 and 4. The resistance of the heating element during operation was measured by an a.c. potentiometric circuit, the details of which were described previously (*15*) along with the calibration procedures. The arrangement of the thermocouples also made it possible to use the thermocouple wires as resistance leads and to measure the temperature distribution on the surface. The calibration

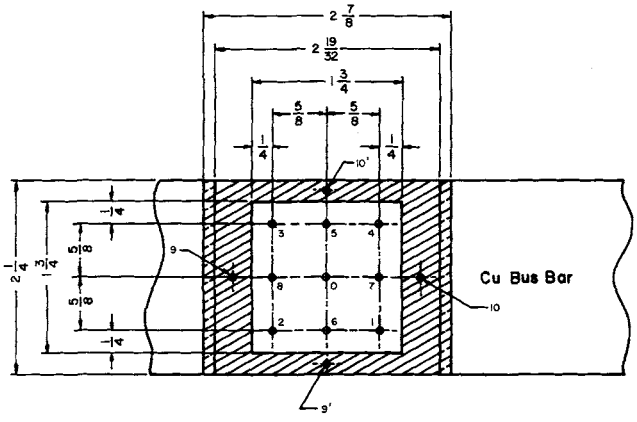

o Location of Thermocouple Junction

Area of Heating Element Under the Gaskets

Silver Solder

Fig. 3. Thermocouple locations and dimensions of heat transfer surface with flat heating elements.

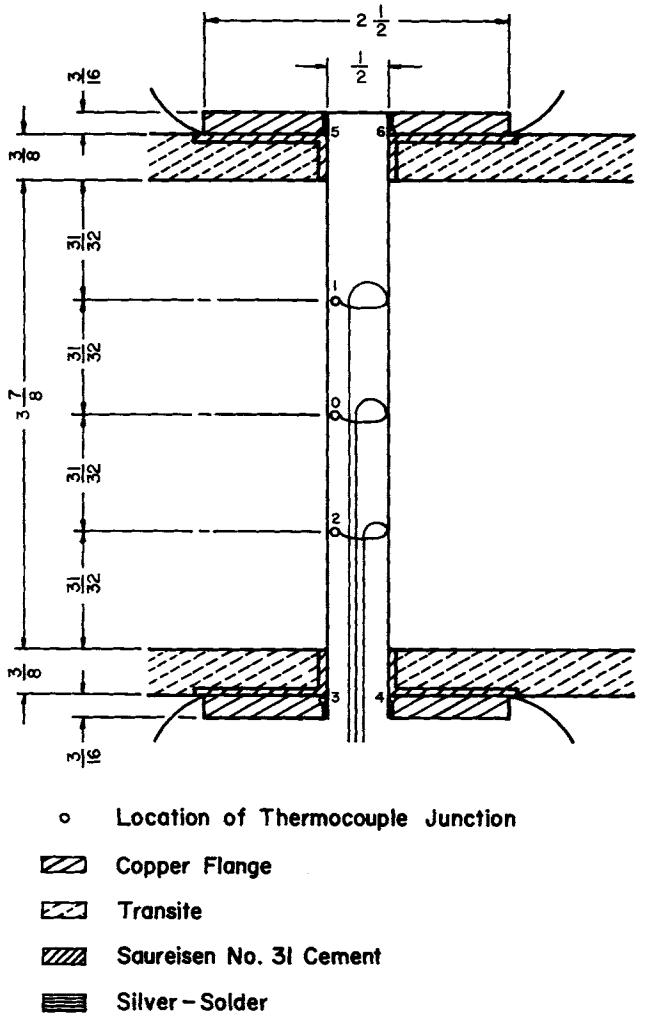

Fig. 4. Thermocouple locations and dimensions of heat transfer surface with tubular heating elements.

of the resistance of the heating elements was checked after every experimental run and, at heat fluxes above 20,000 B.t.u./(hr.)(sq. ft.), it was necessary to recalibrate the resistance between each run because of the slow oxidation of the elements.

The power generation system consisted of a 5-kvamp. voltage stabilizing transformer, a 5.75-kvamp. variac, and a 15/1 step-down transformer. The power input was measured by measuring the current and the voltage drop across the heating element.

OPERATION OF THE EQUIPMENT

The experimental runs were made at approximately constant heat flux over a range of vapor flow rates from zero to the limiting flow rate at which the liquid would tend to break through the heating element, causing unstable operation. The first steady state point of the run was recorded with no vapor suction at low heat fluxes or at a suction rate sufficient to cool the surface down to about 500°F. at the higher heat fluxes. With the asbestos paper flow control elements, the time required to attain steady state was about 20 min. for the first point and less than 10 min. for the subsequent points of the run. With the metallic plate, however, as in the case of ceramic blocks in the previous studies, these periods were more than three times as large, presumably due to small changes in the flow patterns in the flow control elements.

At low flow rates not all the vapor exhausted through the surface, but at higher flow rates very little vapor could be seen coming from the top of the flow control element. As the flow rate was increased, the liquid would approach closer to the heating element, as indicated by the thermocouples attached to the bottom of the element. By calculating the percent of energy input recovered in the exhaust vapor, the fraction of the generated vapor that was sucked through the heating element could be estimated. At the point when all the generated vapor began to flow through the heat source, with the Novabestos-covered tubular heating elements, any further increase in vapor suction rate caused the liquid to break through quickly (in the bottom half of the tube due to the hydrostatic head). But with the metallic plate and also ceramic block flow control elements on a flat heating element, there was an appreciable spread in vapor flow rate between the point where all the vapor entered the element and the point where liquid breakthrough occurred. In fact, in the latter case the temperature read by the central thermocouple was observed to decrease more rapidly with increasing flow rate than the thermocouples on the sides as soon as all the vapor began to flow through the element. However, the operation was very stable; in fact, stable operation (except for slight fluctuations in the thermocouple signals and the a.c. null detector in resistance measured) was possible even with the central thermocouple reading within about 50°F. of liquid temperature. The flow rate at which liquid breakthrough did occur (the central thermocouple reading liquid temperature) was found to be sharply defined. Even a slight decrease from this critical flow rate caused the liquid to recede immediately, but any increase would cause the other thermocouple readings also slowly to reduce to liquid temperature. The exhaust vapor had appreciable superheat even at the critical flow rates, especially at the higher heat fluxes. These observations led to the presumption that liquid would actually tend to enter the heating section at high flow rates, giving a stable evaporation interface in the heating section. Based on this observation, the liquid breakthrough and instability in this operation could be studied theoretically. An approximate model is presented in Part II of this work.

When the Novabestos paper was used as the flow control element on a flat surface, unusually large fluctuations in temperature, pressure drop, and flow rate were observed slightly before the predictable (from the other flow control elements) critical flow rates. It was believed that this was due to the thin flexible asbestos paper, which resulted in increased turbulence in the system and caused appreciable pressure oscillations near the critical flow rates. If, however, the Novabestos paper was held relatively tight against the heat transfer surface (by means of a fiber glass thread with the tubular heating elements or by placing a ¼-in. mesh screen on top of the paper in the case of flat heating elements), these fluctuations were greatly eliminated.

CALCULATION AND ANALYSIS OF DATA

The measured power input was corrected for conduction and radiation losses to calculate the heat flux. No radiation corrections were applied to the power input to the tubular heating elements. Also, no corrections for convection losses were applied to the power input, since it was considered to be a part of the overall heat transfer mechanism. The average surface temperature was calculated by the method used in previous studies (*14, 15*) and involved the following steps: (1) the measured resistance of the heating element was corrected for the area of the heating element under the gasket by using the temperatures read by the thermocouples under the gasket; (2) by using the resistance calibration, the corresponding temperature was noted; and (3) this temperature was corrected for temperature distribution with the thermocouple data to obtain the electrically measured area averaged surface temperature T_{sea}. This latter correction was usually within 2 to 3% of the total temperature driving force.

An error analysis of the data (*17*) indicated that the total relative error in the heat flux was ±5.5%. The maximum error in the calculation of T_{sea} was estimated to be ±15°F at low heat fluxes, but at higher heat fluxes and at high vapor flow rates, this figure was as much as ±30°F. The uncertainty in the measurement of vapor flow rate was less than 1%.

The average heat transfer coefficient h is defined as

$$h = \frac{Q_c}{A(T_{sea} - T_o)} \qquad (1)$$

where Q_c/A is the corrected heat flux and T_o the saturated liquid temperature. Here A is the projected area of the porous heating elements. The heat transfer coefficient and the flow rate were converted into dimensionless numbers by defining a Nusselt number $N_{Nu} = hD/k$ and a Reynolds number $N_{Re} = DG/\mu$, where D is the minimum pore diameter of the heating element, G the superficial mass velocity, and the thermal conductivity k, and viscosity μ of the vapor are evaluated at the saturated vapor temperature.

DISCUSSION OF RESULTS

No Vapor Suction Effect of Flow Control Element

In Figure 5, the heat flux Q_c/A is plotted as a function of average temperature difference $(T_{sea} - T_o)$ for different types of operations. Curves A to E are zero vapor suction curves for different flow control and heating elements. For comparison, the experimental data reported by various investigators for film boiling of liquid nitrogen on solid surface are also given. Curve F was obtained for a flat horizontal surface (*14*); curve G was obtained for a horizontal tube (*18*) and also for a sphere (*19*), whereas curve H was obtained with a vertical tube (*20*). Finally, curves I and J represent approximate instability envelopes for operation with vapor suction by using ceramic blocks and PSS D plate on a flat heating element and Novabestos paper on a tubular heating element, respectively.

Curves A and B, which were obtained in previous studies (*14, 15*) with porous ceramic blocks, show that with no vapor suction, these flow control elements result in a considerably lower heat transfer rate and do not represent desirable operating conditions. The data points obtained in the present work with PSS D flow control element can be seen to be close to curves A and B. If the flow control element is able to bring the liquid close to the heating surface, the heat transfer to liquid can be considerably increased. This is evident from curve E, which was obtained with the two Novabestos-covered tubular heating elements. Curve E shows about a twofold increase in heat transfer rate as compared to normal film boiling and seven- to eightfold increase as compared to zero vapor suction boiling with porous ceramic blocks as flow control elements. This pronounced increase in heat transfer with the thin asbestos paper is evidently due to the high-temperature gradients through the paper which tightly covers the hot surface. It is of interest that Cowley, Timson, and Sawdye (*21*) have shown that by covering a steam-heated copper tube tightly with Vaseline-impregnated asbestos (less than 0.5 mm. thick), an increase in heat transfer rate in film boiling of liquid nitrogen could be obtained.

Curves C and D represent the data points obtained with zero vapor suction by using 1/16 in. asbestos and the Novabestos papers, respectively, on a flat heating surface. Except at lower heat fluxes, a slight effect due to the difference in thickness (and possibly nature) of the papers can be noted. It is further seen from these curves that compared to ceramic blocks, the use of asbestos papers on a flat heating element results in a considerable increase in heat transfer to liquid. However, when compared to curve E, it is also evident that the full capability of the asbestos covering is not achieved in this design. When the thin asbestos paper is placed on top of the flat heating surface of even relatively small area (as in the present design), the vapor flowing upward causes the paper to bulge, which in turn results in a decreased heat transfer to liquid. This is also presumably why curves C and D show a decreased heat transfer rate as compared with boiling on a bare surface (curve

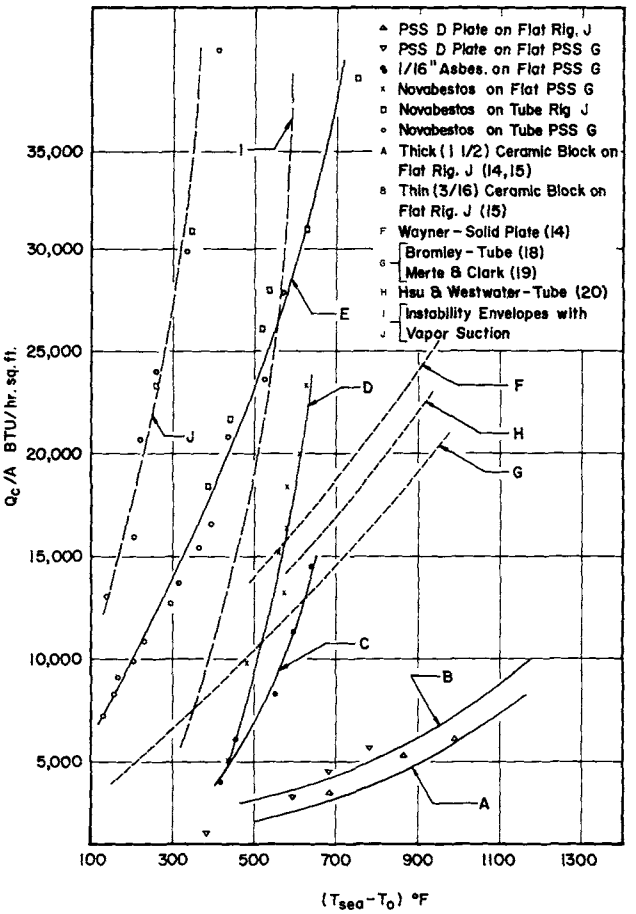

Fig. 5. Comparison of heat flux curves for different types of operation.

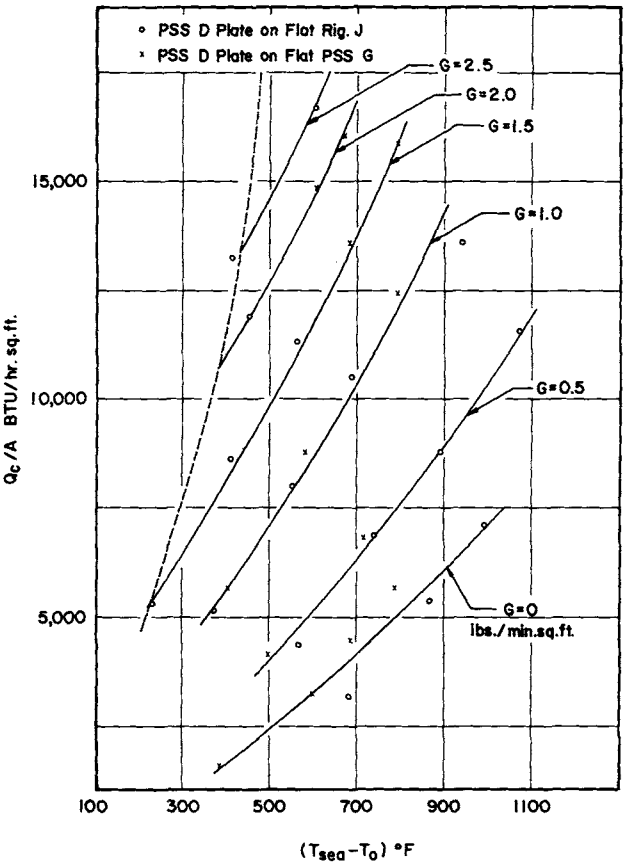

Fig. 6. Heat flux vs. temperature difference for various flow rates with PSS D flow control element on flat heating elements.

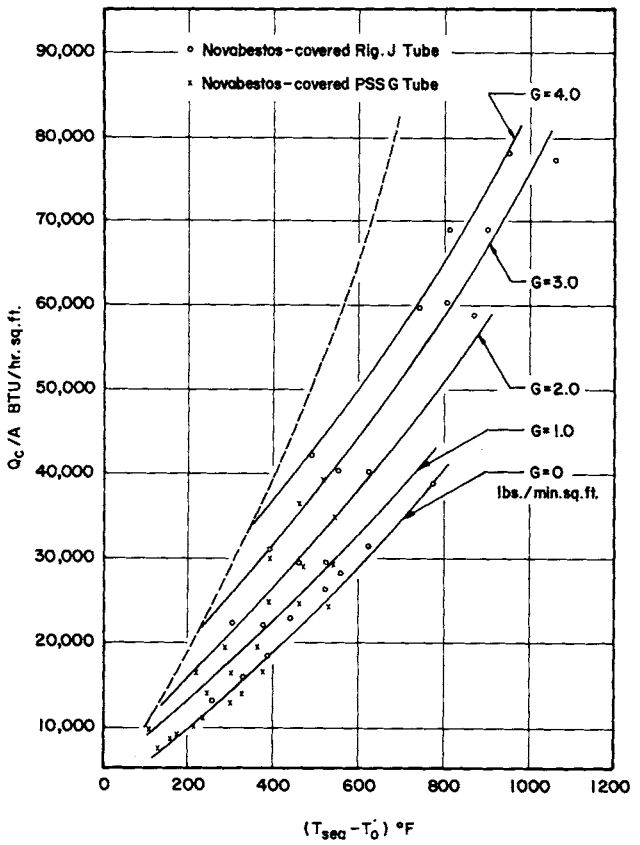

Fig. 7. Heat flux vs. temperature difference for various flow rates with Novabestos-covered tubular heating elements.

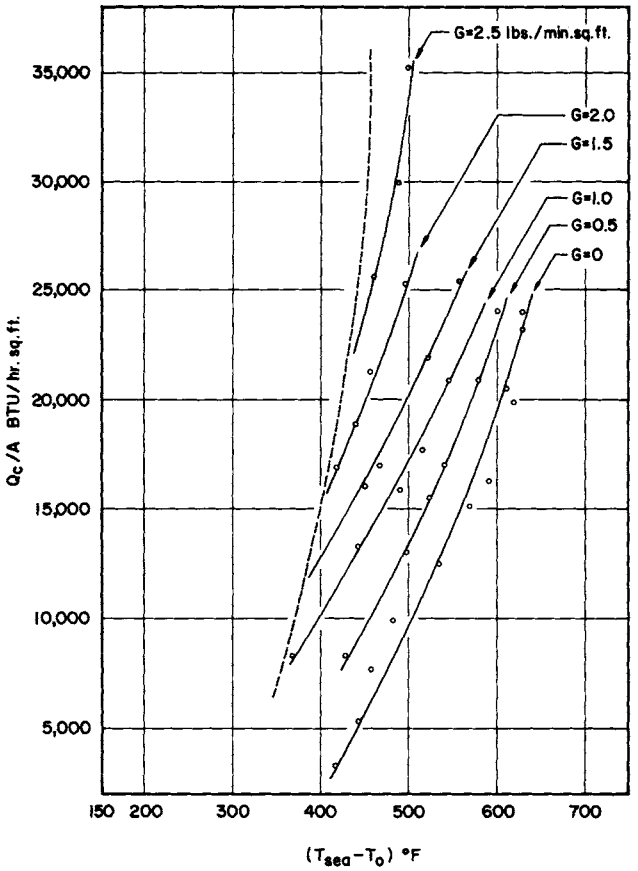

Fig. 8. Heat flux vs. temperature difference for various flow rates with Novabestos-covered PSS G flat heating element.

F) at lower temperature differences. With increasing temperature difference, curve D begins to show a higher heat transfer rate than that given by curve F and also approaches curve E. This is believed to be due to the increased turbulence in the system at higher heat fluxes, which decreases the effective thickness of the vapor film.

The upper limits for heat transfer rate that can be achieved with vapor suction under two different conditions are shown by curves I and J. These represent the heat transfer rates that can be achieved at the critical flow rates. At these flow rates, the liquid tends to penetrate the heating element. At low heat fluxes the liquid would quickly break through the center of the surface, but at higher heat fluxes, sufficient energy is present to vaporize the tongue of liquid in the heating element, thus resulting in a relatively lower surface temperature at the critical flow rates. Curve J represents the maximum heat flux that can be obtained in the present system.

Effect of Vapor Suction

In Figures 6 to 8, the heat flux Q_c/A is plotted as a function of average temperature difference $(T_{sea} - T_o)$ with the superficial mass velocity of vapor through the heating element G as a parameter for the three different systems. The dotted envelopes on the left side are the limits of stable operation. These figures readily demonstrate how vapor suction increases the heat transfer rate in film boiling. The heat transfer coefficient h is plotted as a function of the superficial mass velocity G for the three different systems in Figures 9 to 11. The data with PSS D flow control element on the two different flat heating elements are seen to agree well with the curve for ceramic blocks (Figure 5) obtained previously (*14, 15*). From the point of view of practical application of the system, the use of a porous metallic plate for flow control element seems preferable to porous ceramic blocks. The former makes it possible to have a sandwich construction by using similar materials for flow control and heating elements, which may be more compact and easily fabricated. The heat transfer coefficients obtained with the two Novabestos-covered tubular heating elements are seen to be considerably higher than those obtained with the porous ceramic blocks and metallic plates. The thin

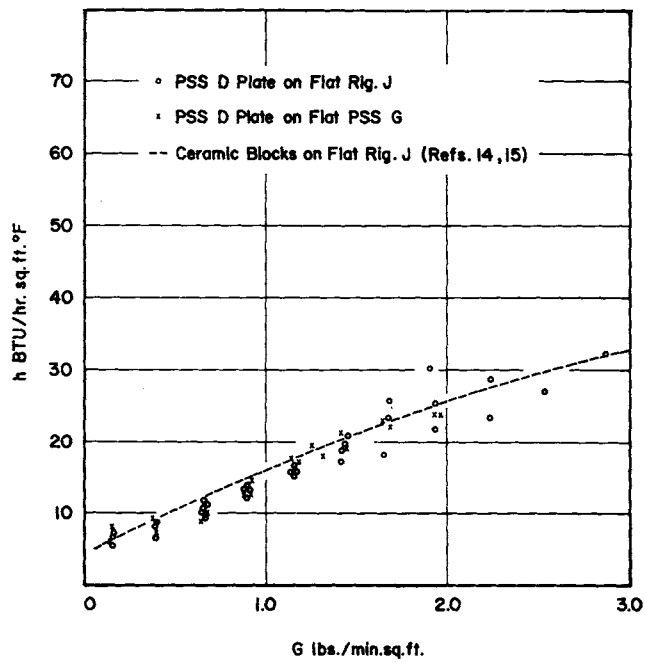

Fig. 9. Heat transfer coefficient vs. vapor flow rate with PSS D flow control element on flat heating elements.

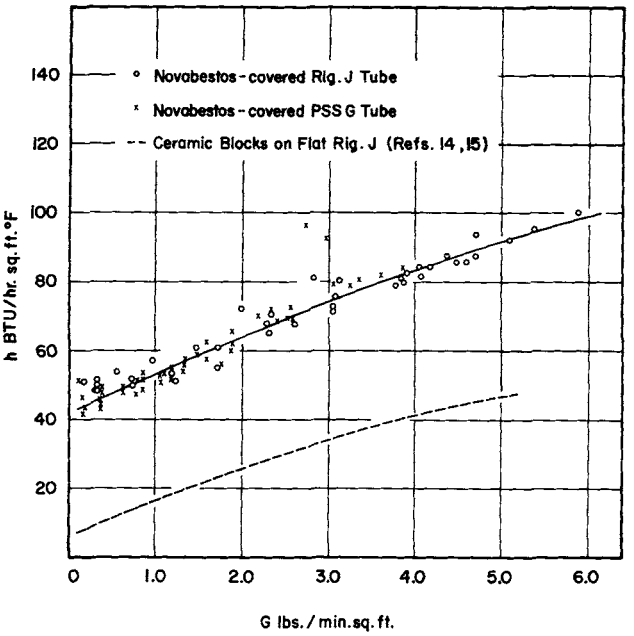

Fig. 10. Heat transfer coefficient vs. vapor flow rate with Novabestos-covered tubular heating elements.

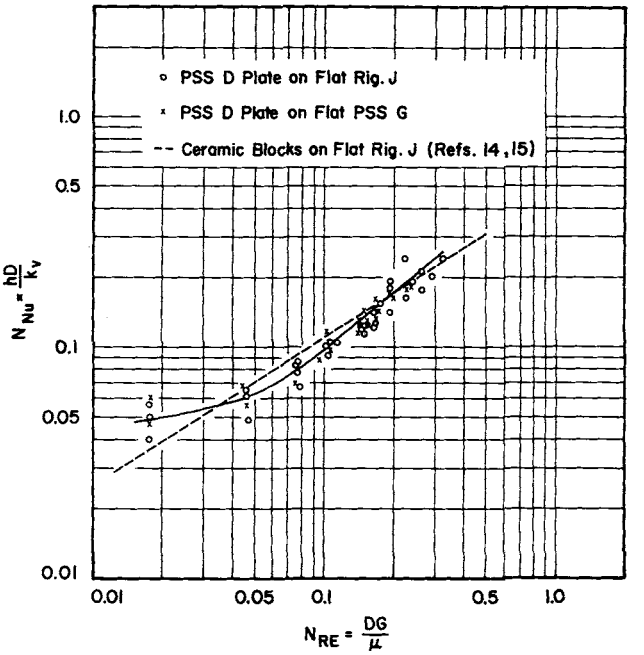

Fig. 12. Nusselt number vs. Reynolds number with PSS D flow control element on flat heating elements.

asbestos paper snugly covering the heating surface brings the liquid closer to the surface than the porous blocks, and the vapor suction results in a pronounced increase in heat transfer rate. With the Novabestos- and 1/16-in. asbestos-covered flat heating elements, the heat transfer coefficients can be seen to be affected by both the vapor flow rate and the level of heat flux. Increase in heat flux presumably causes greater turbulence, as well as motion of the paper, which significantly increases the heat transfer coefficients. By cementing a ¼-in. mesh screen on top of the asbestos paper, the large fluctuations near the critical flow rates were eliminated, but there was still some separation of the paper from the heating surface at low flow rates.

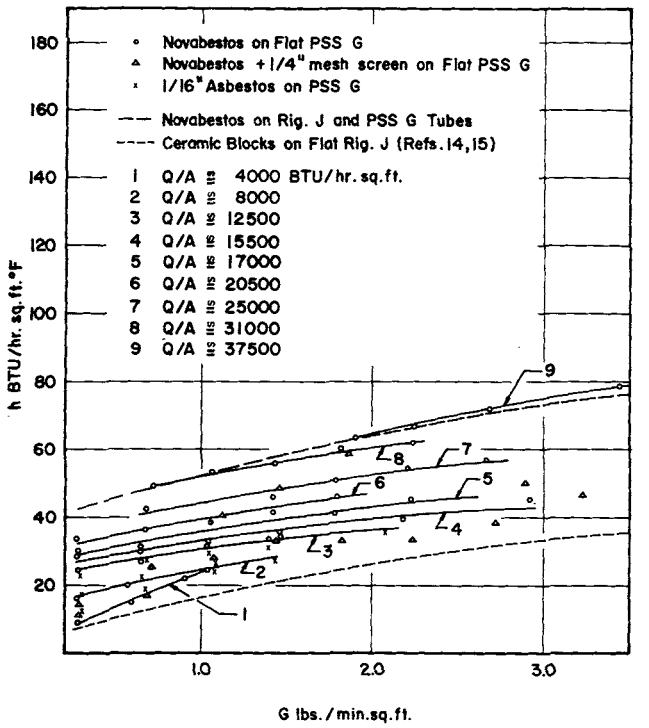

Fig. 11. Heat transfer coefficient vs. vapor flow rate with asbestos-covered flat heating elements.

Dimensionless Correlations

In Figures 12 and 13 the Nusselt numbers are plotted against Reynolds numbers for vapor-suction boiling with PSS D plate on flat heating elements and Novabestos paper on tubular heating elements, respectively. The Nusselt number is a function only of the Reynolds number and the data are correlated by the equation

$$N_{Nu} = 0.044 + 0.925\, N_{Re}^{1.23} \qquad (2)$$

for the PSS D plate on flat heating elements. The data for the Novabestos-covered tubular heating elements are correlated by

$$N_{Nu} = 0.335 + 0.775\, N_{Re}^{1.10} \qquad (3)$$

In Equations (2) and (3) the figures 0.044 and 0.335 represent average values of Nusselt number with zero vapor suction, respectively.

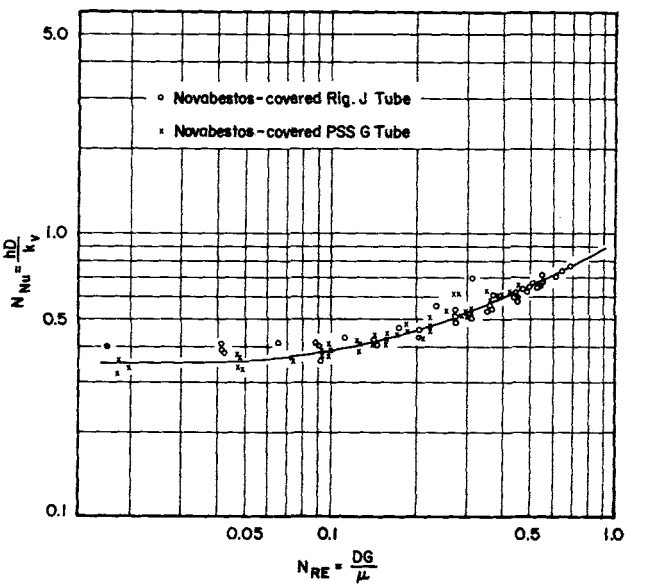

Fig. 13. Nusselt number vs. Reynolds number with Novabestos-covered tubular heating elements.

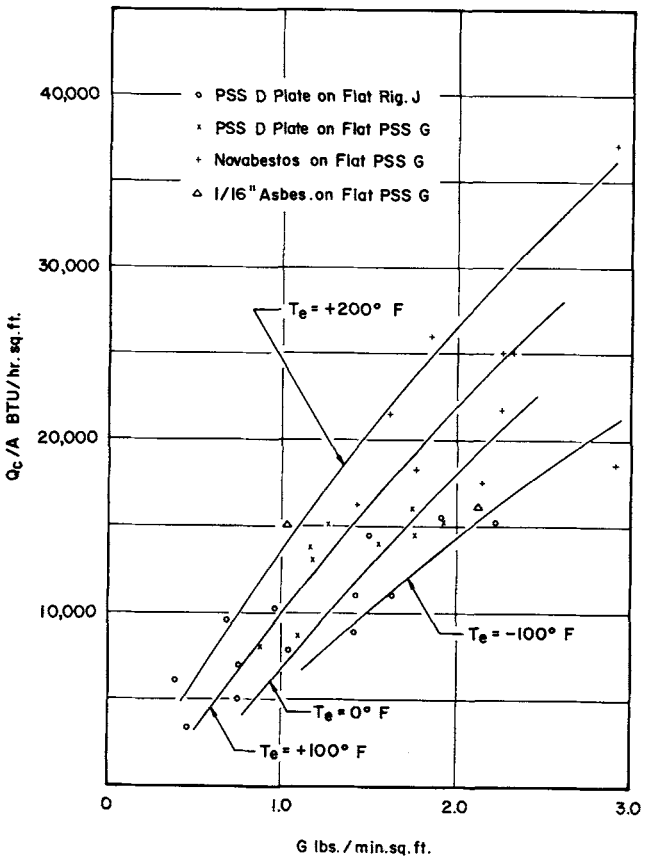

Fig. 14. Heat flux vs. vapor flow rate for various exhaust temperatures with flat heating elements.

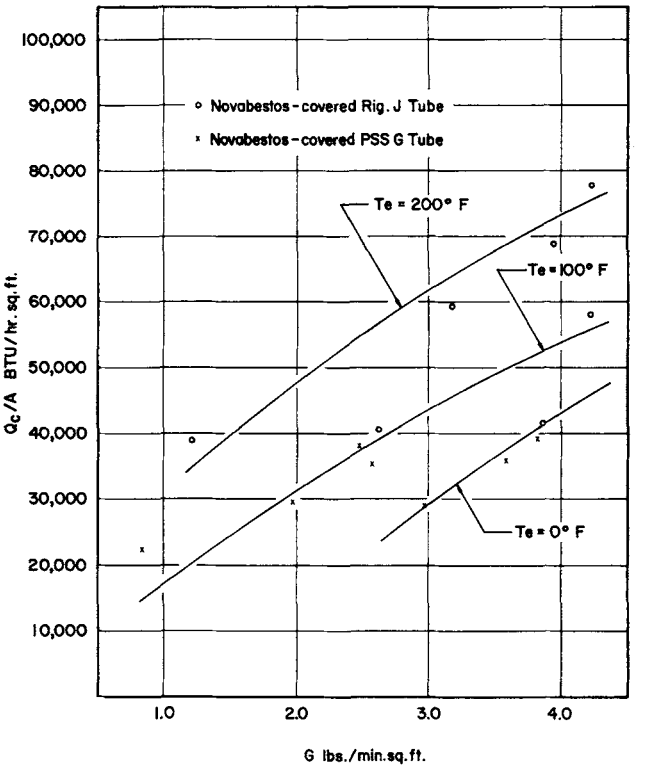

Fig. 15. Heat flux vs. vapor flow rate for various exhaust temperatures with tubular heating elements.

Exhaust Temperature

The heat flux is plotted as a function of the mass velocity of vapor with the exhaust temperature as a parameter in Figures 14 and 15. The measurement of exhaust temperature is subject to errors due to flow of vapor and heat leaks into or out of the exhaust system. At a particular heat flux and flow rate, the exhaust temperature in the case of flat heating elements (Figure 14) is higher than that with the Novabestos-covered tubular heating elements (Figure 15); this is apparently due to the difference in average vapor-film thickness in the two systems, which results in different average surface temperatures. Nevertheless, the advantage of obtaining a superheated vapor by vapor suction boiling is evident.

Pressure Drop

The overall pressure drops through the flow control element, vapor film, and the heating element are plotted against superficial mass velocity through the heating surface in Figures 16 and 17. An accurate measurement of pressure drop in this system is difficult because of change in permeability with temperature and pressure, local corrosion or plugging of heating element, channeling of vapor or liquid, and the possible clogging of the flow control element by ice particles. A considerable scatter in the pressure drop is, therefore, to be expected. Use of the thicker PSS G instead of Rigimesh J heating elements increases the pressure drop. The use of asbestos papers on flat heating elements can be seen to result in considerably higher pressure drop as compared to other systems. This is believed to be due to the clogging of the relatively dense asbestos papers by fine particles suspended in the liquid. That these are principally ice particles is shown by the fact that when the asbestos papers are tightly wrapped around the tubular heating elements, the pres-

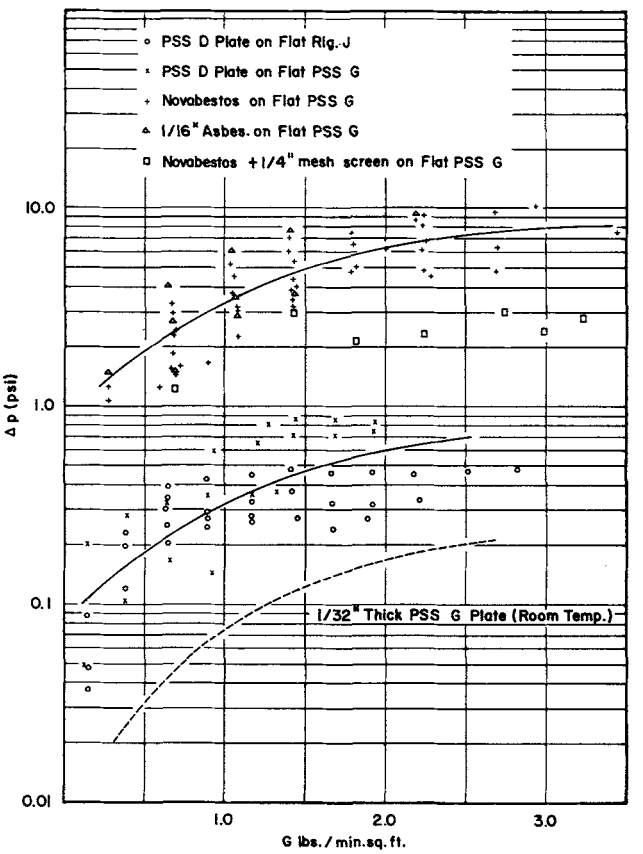

Fig. 16. Pressure drop vs. vapor flow rate with flat heating elements.

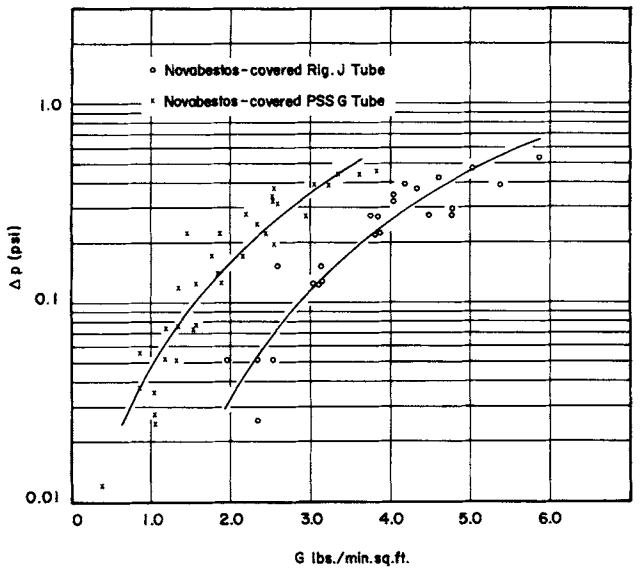

Fig. 17. Pressure drop vs. vapor flow rate with tubular heating elements.

sure drops are relatively low. In this case the asbestos paper is at a much higher temperature than in the case of flat heating elements. In a practical application of this system, the possible clogging of the flow control and/or heating element over a long period of operation is an important point to be considered.

CONCLUDING DISCUSSION

The feasibility of this new mode of boiling heat transfer at heat fluxes twice as high as the peak heat flux in nucleate boiling (*29*) has been established and the results indicate that the method would be applicable at even higher heat fluxes with a more than five times increase in the heat transfer coefficients as compared to normal film boiling. A considerable reduction in the bulk of the flow control element, which is required for the stability of the operation, has been achieved. In fact, the use of very thin asbestos papers is seen to be profitable even at low vapor suction rates. The improvements in heat transfer coefficients added to the superheat obtainable in the exhaust vapor, which could be controlled by changing the vapor flow rate and the heat flux, should make this method of boiling attractive.

An interesting possibility that has not been studied so far in this mode of heat transfer is that, by treating the surface layers of the porous heat source (preferably with a nonwetting substance such as Teflon or a Teflon-asbestos mixture), the flow control element could probably be dispensed with while still obtaining stable operation. That this is possible can be deduced from the fact that a very thin covering of asbestos paper on the heat transfer surface is able to stabilize the system efficiently. Another possibility that may also result in dispensing with the flow control element would be the use of a heating element with a gradient in porosity, decreasing inward from a relatively open structure on the vapor side. It is also interesting to add here that the parallel problem of film condensation on a porous surface with the condensate being sucked through the porous element has been studied theoretically (*22, 23*), showing a substantial increase in heat transfer rate. Experimental work on this problem remains to be done.

ACKNOWLEDGMENT

This work was supported by a grant from the National Science Foundation (G-20224). The assistance of F. L. Maves during the course of this work is gratefully acknowledged. Thanks are also due to Professor Hugh M. Hulburt for his helpful suggestions.

NOTATION

a = thickness of heating element, ft.
A = projected area of process heating element, sq. ft.
A_L = area of heating element covered by liquid tongue, sq. ft.
A_v = area of heating element occupied by vapor, sq. ft.
C = constant potential on the interface, sq. ft./hr.
C_P = specific heat of vapor at constant pressure, B.t.u./(lb.)(°F.)
D = minimum pore diameter, ft.
G = superficial mass velocity, lb./(hr.)(sq. ft.)
G_1 = constant defined by Equation (20A)
k = permeability of heating element, sq. ft.
k_v = thermal conductivity of vapor, B.t.u./(hr.)(°F.)(ft.)
N_{Nu} = hD/k, Nusselt number
N_{Re} = DG/μ, Reynolds number
Δp = pressure drop in heating element, lb./(sq. ft.)(hr.)
q = rate of heat generation, B.t.u./(hr.)(cu. ft.)
Q_c/A = corrected heat flux, B.t.u./(hr.)(sq. ft.)
T_e = average exhaust temperature, °F.
T_o = saturated liquid temperature, °F.
T_{sea} = electrically measured area averaged surface temperature, °F.
U = constant, hr.$^{-1}$
$\vec{V}$ = velocity vector, ft./hr.
w = complex potential, sq. ft./hr.
x = position coordinate, ft.
y = position coordinate, ft.
z = complex variable

Greek Letters

λ = latent heat of vaporization, B.t.u./lb.
μ = viscosity, lb./(ft.)(hr.)
ρ = density, lb./cu. ft.
Φ = potential function, sq. ft./hr.
ψ = stream function, sq. ft./hr.

Subscripts

i = interface
L = liquid
v = vapor

LITERATURE CITED

1. Allingham, W. D., and J. A. McEntire, *J. Heat Transfer*, **83**, 71 (1961).
2. Costello, C. P., and E. R. Redekar *Chem. Eng. Progr. Symposium Ser. No. 41*, **59**, 104 (1963).
3. Costello, C. P., and W. J. Frea, *A.I.Ch.E. J.*, **10**, 393 (1964).
4. Young, R. K., and R. L. Hummel, *Chem. Eng. Progr.*, **60**, No. 7, 53 (1964).
5. Young, R. K., and R. L. Hummel, Preprint No. 38C, A.I.Ch.E. 57th Annual Meeting, Boston, Mass. (1964).
6. Bochirol, E., E. Bonjour, and L. Weil, *Comp. Rend.*, **250**, 76 (1960).
7. Bonjour, E., J. Verdier, and L. Weil, *Chem. Eng. Progr.*, **58**, No. 7, 63 (1962).
8. Markels, Michael, Jr., and R. L. Durfee, *A.I.Ch.E. J.*, **10**, 106 (1964).
9. ————, Preprint No. 38b, A.I.Ch.E. 57th Annual Meeting, Boston, Mass. (1964).
10. Isakoff, S. E., "Heat Transfer and Fluid Mech. Inst.," p. 15, Stanford Univ. Press (1956).
11. DiCicco, D. A., and R. J. Schoenhals, *J. Heat Transfer*, 86, 457 (1964).

12. Pramuk, F. S., and J. W. Westwater, *Chem. Eng. Progr. Symposium Ser. No. 18*, **52**, 75 (1956).
13. Bankoff, S. G., *A.I.Ch.E. J.*, **7**, 485 (1961).
14. Wayner, P. C., Jr., and S. G. Bankoff, *ibid.*, **11**, 59 (1965).
15. Pai, V. K., and S. G. Bankoff, *ibid.*, 65.
16. Wayner, P. C., Jr., and A. S. Kesten, *ibid.*, 858 (1965).
17. Pai, V. K., Ph.D. dissertation, Northwestern Univ., Evanston, Ill. (1965).
18. Bromley, L. A., *Chem. Eng. Progr.*, **46**, 221 (1950).
19. Merte, H., and J. A. Clark, "Advances in Cryogenic Engineering," Academic Press, New York (1961).
20. Hsu, Y. Y., and J. W. Westwater, *A.I.Ch.E. J.*, **4**, 58 (1958).
21. Cowley, C. W., W. J. Timson, and J. A. Sawdye, *Ind. Eng. Chem. Process Design Develop.*, **1**, 81 (1962).
22. Jain, K. C., and S. G. Bankoff, *J. Heat Transfer*, **86**, 481 (1964).
23. Frankel, N. A., and S. G. Bankoff, *ibid.*, **87**, 95 (1965).
24. Saffman, P. G., and Sir Geoffrey Taylor, *Proc. Roy. Soc.*, **245A**, 312 (1957).
25. Saffman, P. G., *Quart. J. Mech. Appl. Math.*, **12**, 146 (1959).
26. Taylor, Sir Geoffrey, and P. G. Saffman, *ibid.*, 265.
27. Scheidegger, A. E., "Physics of Flow Through Porous Media," Toronto Univ. Press, Canada (1950).
28. Collins, R. E., "Flow of Fluids Through Porous Media," Reinhold, New York (1961).

APPENDIX: FILM BOILING FROM POROUS SURFACES WITH VAPOR SUCTION: AN APPROXIMATE MODEL FOR LIQUID BREAKTHROUGH

The experimental observations suggested that the liquid breakthrough in the heating section could be studied theoretically by assuming a stable evaporation interface in the porous element, which would move along the depth of the section as the flow rate was increased. The problem becomes mainly one of obtaining an equation which describes this stable interface as a function of the variables, namely, heat input (q), pressure drop (Δp), and flow rate (G). This equation would then define the conditions under which the liquid breakthrough would begin. An approximate solution to the problem is presented here which consists essentially of assuming a complex potential to describe the flow pattern in the system which would define, under suitable assumptions, a tongue-shaped evaporation interface.

It is of interest to note here that an analogous problem of motion of an interface between two immiscible fluids in a porous medium due to the instability which occurs when the penetrating fluid is less viscous has been studied in detail, among others, by Taylor and Saffman (*24* to *28*). The present problem is complicated by the phase change occurring at the interface and the finite depth of the porous heating section.

Figure 18 represents the theoretical model under consideration. Liquid is fed uniformly into a heat producing porous section of thickness a, by a similar although nonheat generating, porous medium which extends to infinity. The latter represents the flow control element in the experiments and its thickness is assumed to have negligible influence on the conditions for liquid breakthrough in the heating section.

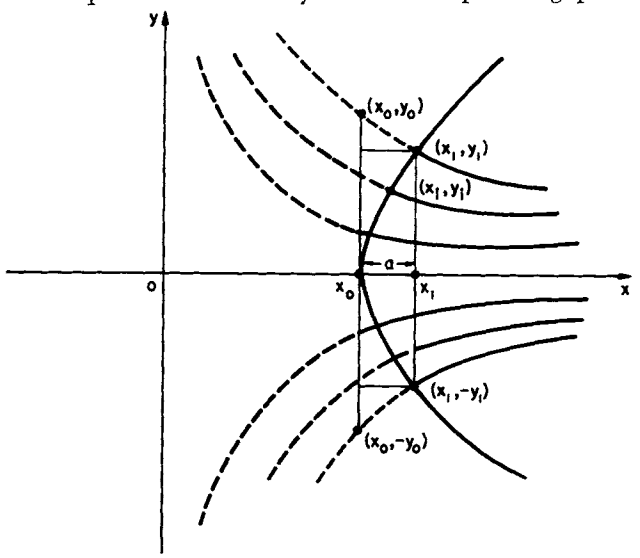

Fig. 18. Flow pattern in the theoretical model.

The flow pattern in the porous medium is assumed to be described by the complex potential given by

$$w = \Phi + i\psi = Uz^2; z = x + iy \tag{1A}$$

where U is a constant with the dimension of reciprocal time. The choice of this function makes it possible to define conveniently a tongue-shaped evaporation interface as described below. It is assumed that $(x_1 - x_0)/x_0 << 1$. The streamlines and the constant potential lines are given by

$$\psi = 2Uxy; \Phi = U(x^2 - y^2) \tag{2A}$$

If the flow system obeys Darcy's law, the pressure drop in the liquid phase in the heating section can then be neglected as compared with that in the vapor phase, since the kinematic viscosity of the vapor is large compared to that of liquid. Applying Darcy's law, one obtains

$$\vec{V} = \nabla\Phi = -\frac{k}{\mu}\nabla p \tag{3A}$$

so that the evaporation interface, as a constant pressure surface, and hence a constant potential surface, is described by a hyperbolic shape. These constant-potential surfaces are imagined to be liquid tongues entering the heating section.

The surface $\Phi = C$ is now assumed to represent the liquid tongue which has just reached the depth of the heating section. The uniform superficial mass velocity of the liquid entering the section is

$$G = 2Ux_1\rho_L \tag{4A}$$

and since $\Phi = C$ on the interface, Equation (2A) gives

$$C = U(x_1^2 - y_1^2) = Ux_0^2 \tag{5A}$$

Further, a heat balance in the liquid phase gives

$$qA_L = 2Gy_1\lambda \tag{6A}$$

Equation (6A) assumes negligible thermal conductivity of the porous medium. By using the equation for the interface, the area A_L is given by

$$A_L = x_1\left(x_1^2 - \frac{C}{U}\right)^{1/2} + \frac{C}{U}\left[\ln\left[\frac{(C/U)^{1/2}}{x_1 + \left(x_1^2 - \frac{C}{U}\right)^{1/2}}\right]\right] \tag{7A}$$

so that Equation (6A) becomes

$$q = \frac{2G\lambda}{x_1 + \frac{C}{U\left(x_1^2 - \frac{C}{U}\right)^{1/2}}\ln\left[\frac{(C/U)^{1/2}}{x_1 + \left(x_1^2 - \frac{C}{U}\right)^{1/2}}\right]} \tag{8A}$$

Since the depth of the heating section is known, use of Equation (5A) gives

$$x_0 = x_1 - a \text{ or } \frac{C}{U} = (x_1 - a)^2 \tag{9A}$$

The potential Φ' and stream function ψ' in the vapor phase are now defined by

$$\Phi' = \frac{\rho_L U}{\rho_v}(x^2 - y^2); \psi' = \frac{2\rho_L Uxy}{\rho_v} \tag{10A}$$

so that the mass balance across the interface is satisfied. On the interface Φ' satisfies

$$\Phi' = \frac{\rho_L C}{\rho_{vi}} \tag{11A}$$

where ρ_{vi} is the saturation density of the vapor. The average value of Φ' on the plane $x = x_0$ is given by

$$\Phi' |_{x = x_0} = \frac{\rho_L U}{y_0} \int_0^{y_0} \frac{x_0^2 - y^2}{\rho_v} dy \qquad (12A)$$

The pressure drop through the heating section is thus

$$\frac{k}{\mu} \Delta p = \frac{\rho_L C}{\rho_{vi}} - \frac{\rho_L U}{y_0} \int_0^{y_0} \frac{x_0^2 - y^2}{\rho_v} dy \qquad (13A)$$

If the thickness of the heating element is small, as in the experimental work done to date, the change in ρ_v can be neglected and $y_1 \approx y_0$. Using Equation (5A) one can simplify Equation (13A) to

$$x_1^2 - \frac{C}{U} = 3 \frac{k}{\mu} \frac{\rho_{vi}}{\rho_L} \frac{\Delta p}{U} \qquad (14A)$$

Combination of Equations (4A), (8A), (9A), and (14A) results in

$$x_1 = \frac{aG}{2\left(G - 3\frac{k}{\mu} \rho_{vi} \frac{\Delta p}{a}\right)} \qquad (15A)$$

$$q = \frac{2G\lambda}{x_1 + \frac{(x_1 - a)^2}{(2ax_1 - a^2)^{1/2}} \ln\left(\frac{x_1 - a}{x_1 + (2ax_1 - a^2)^{1/2}}\right)} \qquad (16A)$$

These two equations together give the desired relation between heat input, pressure drop, and flow rate at which the liquid will begin to break through the heating section.

It is further noted that the average superheat in the vapor leaving the section when the liquid begins to break through is given by

$$2Gy_1 C_p (T_e - T_o) = qA_v \qquad (17A)$$

Using Equations (7A) and (8A), one can rewrite Equation (17A) as

$$qa = G\lambda + G C_p (T_e - T_o) \qquad (18A)$$

which gives the overall heat balance in the system.

Discussion

Liquid breakthrough in the heating element can occur in two distinct ways: complete breakthrough and local breakthrough. Complete breakthrough, by definition, occurs when the heating element is just completely filled with liquid before any liquid breaks through it. The critical flow rate is then given by the heat balance equation $G\lambda = qa$. On the other hand, local breakthrough occurs when a tongue of liquid begins to dip through the heating section locally at the center, so that at this point liquid occupies the least area in the heating section, and consequently the exhaust vapor at the critical flow rate may still have considerable superheat. At a given heat flux, the critical flow rate is obviously maximum if the breakthrough is complete. If the breakthrough is local, however, the critical flow rate may vary over a wide range, depending on the shape of the liquid tongue.

Equations (15A) and (16A) can be rewritten, solving for qa, to give

$$qa = \frac{2G\lambda}{\frac{G}{2(G - G_1)} + \frac{(2G_1 - G)^2}{4[G_1(G - G_1)^3]^{1/2}} \ln\left(\frac{2G_1 - G}{G + 2[G_1(G - G_1)]^{1/2}}\right)} \qquad (19A)$$

where

$$G_1 = 3\frac{k}{\mu} \rho_{vi} \frac{\Delta p}{a}; \; x_1 = \frac{aG}{2(G - G_1)} \qquad (20A)$$

The value of x_1 in the analysis could vary between a and ∞ and the basewidth and the shape of the tongue vary accordingly. When $x_1 = a$, Equations (19A) and (20A) give

$$G = 6\frac{k}{\mu} \rho_{vi} \frac{\Delta p}{a} \qquad (21A)$$

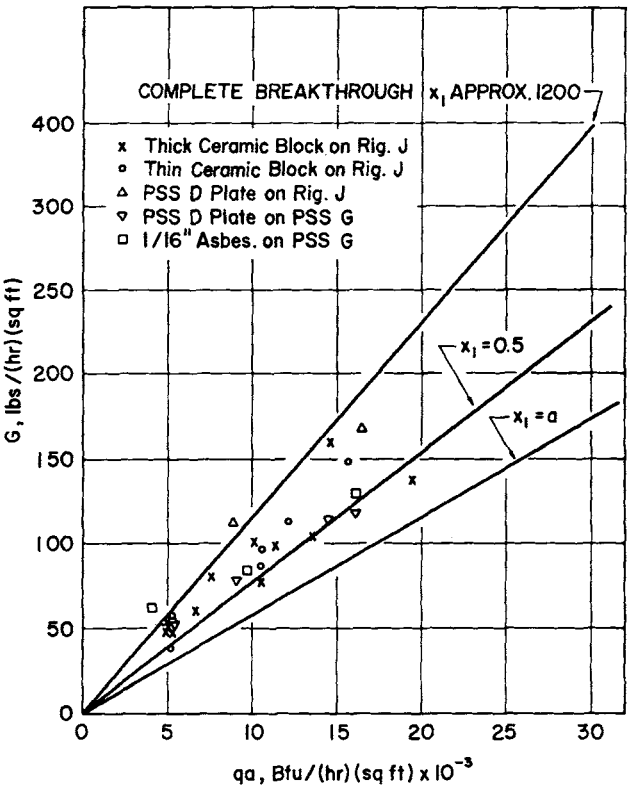

Fig. 19. Critical flow rate vs. heat flux for various values of x_1 compared with experimental data.

and

$$qa = 2G\lambda \qquad (22A)$$

This gives the lower limit on the critical flow rate in local breakthrough and it is equal to half the complete breakthrough flow rate (qa/λ). The shape of the liquid tongue is triangular at this point, which is a consequence of the choice of the complex potential. At the other extreme, $x_1 = \infty$, so that $G = G_1$ and the heat input is zero. It is possible then at some value of x_1 to have the condition for complete breakthrough satisfied. This value of x_1 is given [by putting $q = G\lambda/a$ in Equation (16)]

$$x_1 + \frac{(x_1 - a)^2}{(2ax_1 - a^2)^{1/2}} \ln\left(\frac{x_1 - a}{x_1 + (2ax_1 - a^2)^{1/2}}\right) = 2a \qquad (23A)$$

In Figure 19 the critical flow rate is plotted as a function of heat flux (qa) for different values of x_1, along with the experimentally observed liquid breakthrough points for the Rigimesh J and PSS G heating elements by using ceramic blocks, PPS D plate, and 1/16-in. asbestos paper as the flow control elements. At a given heat flux the value of x_1 in the model determines the shape of the liquid tongue and the corresponding critical flow rate, which is bounded by the upper limit (complete breakthrough) and lower limit (local breakthrough). The experimental points are seen to be appreciably above the lower limit of local breakthrough given by $x_1 = a$ in the model. At low heat fluxes, the breakthrough is close to complete, whereas at higher heat fluxes, appreciable deviations for complete breakthrough can be seen. It is to be noted, however, that at higher heat fluxes, the edge effects may become appreciable.

Manuscript received January 10, 1966; revision received April 7, 1966; paper accepted April 13, 1966.